OXFORD

Human Molecular Genetics, 2018, Vol. 27, No. 14 2502–2516

doi: 10.1093/hmg/ddy154
Advance Access Publication Date: 25 April 2018
Original Article

ORIGINAL ARTICLE

Mutant APP and amyloid beta-induced defective autophagy, mitophagy, mitochondrial structural and functional changes and synaptic damage in hippocampal neurons from Alzheimer's disease

P. Hemachandra Reddy[1,2,3,4,5,6,7,*], XiangLing Yin[1], Maria Manczak[1], Subodh Kumar[1], Jangampalli Adi Pradeepkiran[1], Murali Vijayan[1] and Arubala P. Reddy[1,8]

[1]Garrison Institute on Aging, [2]Garrison Institute on Aging, South West Campus, [3]Cell Biology & Biochemistry Department, [4]Pharmacology & Neuroscience Department, [5]Neurology Department and [6]Speech, Language and Hearing Sciences Department, Texas Tech University Health Sciences Center, Lubbock, TX 79430, USA, [7]Department of Public Health, Graduate School of Biomedical Sciences, Lubbock, TX 79430, USA and [8]Department of Internal Medicine, Texas Tech University Health Sciences Center, Lubbock, TX 79430, USA

*To whom correspondence should be addressed at: Mildred and Shirley L. Garrison Chair in Aging, Neuroscience & Pharmacology and Neurology Departments, Texas Tech University Health Sciences Center, 3601 Fourth Street/MS/9424/4A 124, Lubbock, TX 79430, USA.
Tel: 806-743-2393; Fax: 806-743-3636; Email: hemachandra.reddy@ttuhsc.edu

Abstract

The purpose of our study was to determine the toxic effects of hippocampal mutant APP (mAPP) and amyloid beta (Aβ) in human mAPP complementary DNA (cDNA) transfected with primary mouse hippocampal neurons (HT22). Hippocampal tissues are the best source of studying learning and memory functions in patients with Alzheimer's disease (AD) and healthy controls. However, investigating immortalized hippocampal neurons that express AD proteins provide an excellent opportunity for drug testing. Using quantitative reverse transcriptase-polymerase chain reaction, immunoblotting & immunofluorescence and transmission electron microscopy, we assessed messenger RNA (mRNA) and protein levels of synaptic, autophagy, mitophagy, mitochondrial dynamics, biogenesis, dendritic protein MAP2 and assessed mitochondrial number and length in mAPP-HT22 cells that express Swedish/Indiana mutations. Mitochondrial function was assessed by measuring the levels of hydrogen peroxide, lipid peroxidation, cytochrome c oxidase activity and mitochondrial adenosine triphosphate. Increased levels of mRNA and protein levels of mitochondrial fission genes, Drp1 and Fis1 and decreased levels fusion (Mfn1, Mfn2 and Opa1) biogenesis (PGC1α, NRF1, NRF2 & TFAM), autophagy (ATG5 & LC3BI, LC3BII), mitophagy (PINK1 & TERT, BCL2 & BNIPBL), synaptic (synaptophysin & PSD95) and dendritic (MAP2) genes were found in mAPP-HT22 cells relative to WT-HT22 cells. Cell survival was significantly reduced mAPP-HT22 cells. GTPase-Drp1 enzymatic activity was increased in mAPP-HT22 cells. Transmission electron microscopy revealed significantly increased mitochondrial numbers and reduced mitochondrial length in mAPP-HT22 cells. These findings suggest that hippocampal accumulation of mAPP and Aβ is responsible for abnormal mitochondrial dynamics and defective biogenesis, reduced MAP2, autophagy, mitophagy and synaptic proteins & reduced dendritic spines and mitochondrial structural and functional changes in mAPP hippocampal cells. These

Received: March 7, 2018. **Revised:** April 15, 2018. **Accepted:** April 23, 2018

observations strongly suggest that accumulation of mAPP and Aβ causes mitochondrial, synaptic and autophagy/mitophagy abnormalities in hippocampal neurons, leading to neuronal dysfunction.

Introduction

Alzheimer's disease (AD) is age-related, multifactorial neurodegenerative disease, characterized by memory loss and multiple cognitive changes (1). As people age, memory and the ability to carry out tasks often decline and their risk for neuronal damage increases. AD occurs in two forms—early-onset familial and late-onset sporadic (2). In early-onset AD, genetic mutation is responsible for clinical symptoms and disease process, whereas in late-onset, age-related factors are responsible for disease process and clinical symptoms (2). According to the *World Alzheimer's Report*, in 2016, over 46.8 million people worldwide had one of the forms of AD, and it projects that this number will increase to more than 131 million by 2050 and the total estimated annual worldwide health care costs for persons with AD was $818 billion in 2016 (3). With increased lifespan of humans, AD is a major health concern in the society.

Pathological and morphological studies of postmortem AD brains and brain tissues from AD mouse models revealed that intracellular neurofibrillary tangles, extracellular neuritic plaques or Aβ deposits are major pathological changes, in addition to synaptic damage, loss of synaptic proteins, proliferation of reactive astrocytes and activated microglia, defects in cholinergic neurons, an age-dependent imbalance in hormones and structural and functional changes in mitochondria (4–10). Among these changes, synaptic damage and mitochondrial damage are widely recognized as early events in the pathogenesis of AD (Reddy *et al*., 2012). The loss of synapses and synaptic damage are the best correlates of cognitive decline found in AD patients.

Histological and anatomical examination of autopsied AD brains revealed that a neurodegenerative process is initiated in layer 2 of the entorhinal cortex and spreads to the hippocampus, temporal cortex, fronto-parietal cortex and finally to subcortical nuclei (11–13). Further, in the progression of disease, the association between the entorhinal cortex and the hippocampal dentate gyrus becomes disconnected, and later on, neuronal connections within hippocampal regions (CA3, CA1 and subiculum) become disconnected (13). These degenerative changes that occur in brain regions are responsible for learning, memory and cognitive problems in AD patients.

Hippocampus is a major component in the brains of mammals, including humans. There are two hippocampi, one in each side of the brain and plays important roles in the consolidation of information from short-term memory to long-term memory, and in spatial memory that enables navigation. A short-term memory loss and disorientation are the early symptoms in AD (14–16). Recent research also revealed that the hippocampus plays a critical role in the formation, organization and storage of new memories as well as connecting certain sensations and emotions to these memories (14–16). Studies also suggest that greater hippocampal activity during sleep following training or learning experience leads to better memory of the material the following day. Hippocampal structure and function can be studied by genes/proteins that express in hippocampal neurons in rodent models of AD and autopsied brains from healthy subjects and AD patients.

Hippocampal tissues are the best source of studying learning and memory functions in cognitively intact healthy subjects and patients with different stages of dementia. However, investigating hippocampal neurons, particularly immortalized neurons will provide an excellent opportunity for testing normal and disease states and also assessing drug targets. Several groups, worked on immortalized mouse primary hippocampal neurons 'referred HT22 cells'. These cells were originally subcloned from the hippocampal cell line (HT-4) (17). The parental HT-4 cell line was derived from the immortalization of mouse hippocampal tissues with a temperature sensitive SV40 T-antigen (18).

We recently studied the toxic effects of hippocampal mAPP and Aβ in 12-month-old APP transgenic mice (19). Using rotarod and Morris water maze tests, immunoblotting & immunofluorescence, Golgi-cox staining and transmission electron microscopy, we assessed cognitive behavior, protein levels of synaptic, autophagy, mitophagy, mitochondrial dynamics, biogenesis, dendritic protein MAP2 and quantified dendritic spines and mitochondrial number and length in 12-month-old APP mice with Swedish mutation. Mitochondrial function was assessed by measuring the levels of hydrogen peroxide (H_2O_2), lipid peroxidation, cytochrome coxidase activity and mitochondrial adenosine triphosphate (ATP). Morris water maze and rotarod tests revealed that hippocampal learning and memory and motor learning & coordination were impaired in APP mice relative to wild-type (WT) mice. Increased levels of mitochondrial fission proteins, and decreased levels fusion, autophagy, Mitophagy, synaptic and dendritic proteins were found in 12-month-old APP mice relative to WT mice. Golgi-cox staining analysis revealed that dendritic spines are significantly reduced. Transmission electron microscopy revealed significantly increased mitochondrial numbers and reduced mitochondrial length in APP mice. These findings suggest that hippocampal accumulation of mAPP and Aβ is responsible for abnormal mitochondrial dynamics and defective biogenesis, reduced dendritic spines and hippocampal based learning and memory impairments and mitochondrial structural and functional changes in APP mice.

In this study, we sought to determine messenger RNA (mRNA) and protein levels of mitochondrial dynamics, biogenesis, dendritic, synaptic and mitophagy/autophagy genes in the mouse primary hippocampal (HT22) cells transfected and untransfected with mAPP complementary DNA (cDNA) (with Swe/Indiana mutations). We also assessed cell survival, GTPase-Drp1 enzymatic activity, mitochondrial function and ultrastructural changes.

Results

Full-length mutant APP and soluble Aβ levels

To determine the transfection efficiency of mAPP cDNA in HT22 cells, we performed immunoblotting analysis of cell pellets of HT22 cells transfected and untransfected with mAPP cDNA and using 6E10 antibody that recognizes mutant full-length APP. Using sandwich ELISA, we also measured soluble Aβ40 and 42 levels.

As shown in Figure 1A, we found 110 kDa full-length mAPP in lane 2 that represents protein lysates from HT22 cells transfected with mAPP cDNA, but not in lane 1 that represents untransfected HT22 cells.

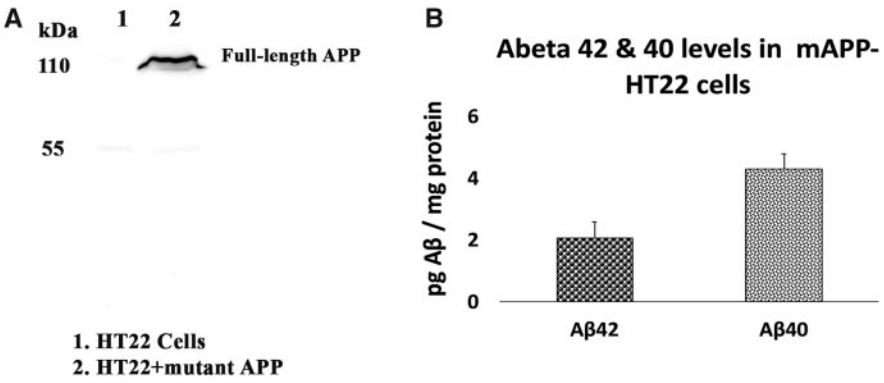

Figure 1. Immunoblotting analysis and soluble Aβ levels in HT22 cells transfected with mutant APP cDNA. Figure 1A shows representative immunoblotting analysis of mutant APP-HT22 cells. Mouse primary hippocampal (HT22) cells were transfected with mutant APP cDNA (with Swe/Indiana mutations) for 48 h and cells were harvested and protein lysates were made and resolved on 4–20 gradient gel and probed with 6E10 antibody that recognizes full-length mutant APP. A-110 mutant full-length APP protein was found in mutant APP-HT22 cells, but not in untransfected HT22 cells. Figure 1B shows Aβ42 and 40 levels in HT22 cells transfected with mutant APP cDNA.

Our sandwich ELISA assay revealed that increased Aβ42 levels compared to Aβ40, with a ratio of 0.48/1.0 Aβ42/Aβ40 in HT22 cells transfected with mAPP cDNA.

mRNA and protein levels

To understand the effects of mAPP and Aβ on mitochondrial dynamics, biogenesis, synaptic, autophagy and dendritic proteins in HT22 cells transfected and untransfected with mAPP cDNA, we performed real-time qRT-PCR and immunoblotting analysis assessed mRNA levels and protein levels of mitochondrial fission, fusion, biogenesis, synaptic and autophagy and mitophagy proteins.

Gene expression differences between mutant APP-HT22 cells and untransfected HT22 cells

To determine the effects of hippocampal mAPP and Aβ on mitochondrial dynamics, biogenesis, autophagy, mitophagy and synaptic genes, we measured mRNA levels of mitochondrial dynamics, biogenesis, autophagy, mitophagy and synaptic genes using real-time reverse transcriptase-polymerase chain reaction (RT-PCR).

Mitochondrial dynamics genes

We found significantly increased levels of mRNA expression levels of fission genes Drp1 (by 2.1-fold) and Fis1 (by 1.7-fold) in mAPP-HT22 cells relative to untransfected, WT-HT22 cells (Table 1). In contrast, the levels of mRNA expression of the mitochondrial fusion genes Mfn1 (by 1.8-fold), Mfn2 (by 2.2-fold) and Opa1 (by 1.9-fold) reduced in mAPP-HT22 cells. These findings indicate that hippocampal mAPP and Aβ increase fission activity and reduce fusion activity hippocampal cells.

Synaptic genes

Significantly decreased mRNA expression levels were found in synaptic genes, synaptophysin (by 2.2-fold), PSD95 (by 3.1-fold) in mAPP-HT22 cells relative to untransfected, WT-HT22 cells, indicating that hippocampal mAPP and Aβ reduce synaptic activities (Table 1).

Biogenesis genes

Significantly reduced mRNA levels were found in PGC1α (by 2.1-fold), NRF1 (by 1.8-fold), NRF2 (by 1.6-fold) and TFAM (by 2.5-fold) in mAPP-HT22 cells relative to untransfected, WT-HT22 cells, suggesting that hippocampal mAPP and Aβ decrease mitochondrial biogenesis (Table 1).

Table 1. Fold changes of mRNA expression of mitochondrial structural, synaptic, biogenesis, autophagy and mitophagy genes in mutant APP-HT22 cells compared to untransfected WT-HT22 cells

	Genes	mRNA fold changes in mutant HT22 cells
Mitochondrial structural genes	Drp1	2.1**
	Fis1	1.7*
	Mfn1	−1.8*
	Mfn2	−2.2*
	OPA1	−1.9*
Synaptic genes	Synaptophysin	−2.2**
	PSD95	−3.1**
Biogenesis gens	PGC1α	−2.1**
	Nrf1	−1.8*
	Nrf2	−1.6*
	TFAM	−2.5**
Autophagy genes	LC3A	−1.6*
	LC3B	−1.8*
	ATG5	−2.5
	Beclin1	−1.5*
Mitophagy genes	PINK1	−2.4**
	TERT	−2.1**
	BCL2	−1.5*
	BNIP3L	−1.3

*P<0.05; **P<0.005.

Autophagy and mitophagy genes

Significantly reduced mRNA levels were found in autophagy genes ATG5 (by 2.5-fold), Beclin 1 (by 1.5-fold), LC3A (by 1.6-fold), LC3B (by 1.8-fold), and mitophagy genes PINK1 (by 2.4-fold), TERT (by 2.1-fold), BCL2 (by 1.5-fold) and BNIP3L (by 1.3-fold) in mAPP-HT22 (Table 1).

Immunoblotting analysis

To determine the toxic effects of mAPP and Aβ on protein levels, we performed immunoblotting analysis of protein lysates prepared from mAPP-HT22 cells and untransfected, WT-HT22 cells. As shown in Figure 1, we found 110 kDa full-length APP in

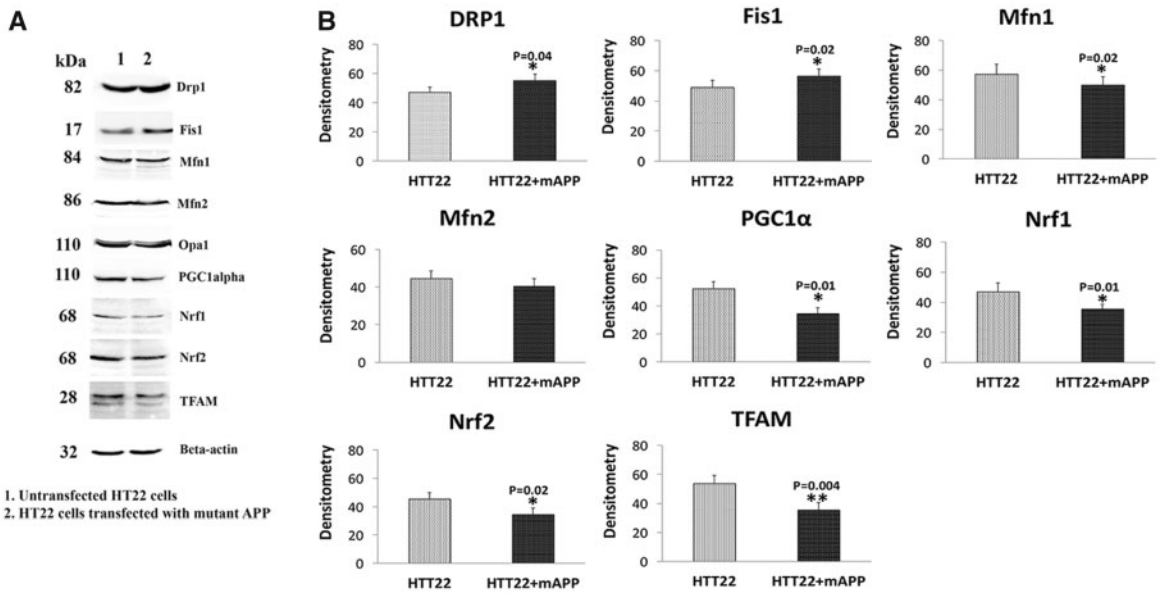

Figure 2. Immunoblotting analysis of mitochondrial dynamics and biogenesis proteins in mutant APP-HT22 cells. Figure 2A and 2B shows representative immunoblots of HT22 cells transfected and untransfected with mutant APP cDNA. Figure 2B shows quantitative densitometry analysis of mitochondrial dynamics—Drp1, Fis1 (fission), Mfn1, Mfn2 and Opa1 (fusion) and biogenesis (PGC1α, NRF1, NRF2 and TFAM) proteins. Fission proteins Drp1 ($P=0.04$) and Fis1 ($P=0.02$) were significantly increased and fusion protein Mfn1 ($P=0.02$) significantly reduced in mutant APP-HT22 cells relative to untransfected HT22 cells. Mitochondrial biogenesis proteins—PGC1α ($P=0.01$), NRF1 ($P=0.01$), NRF2 ($P=0.02$) and TFAM ($P=0.004$) were significantly reduced in mutant APP-HT22 cells relative to untransfected HT22 cells.

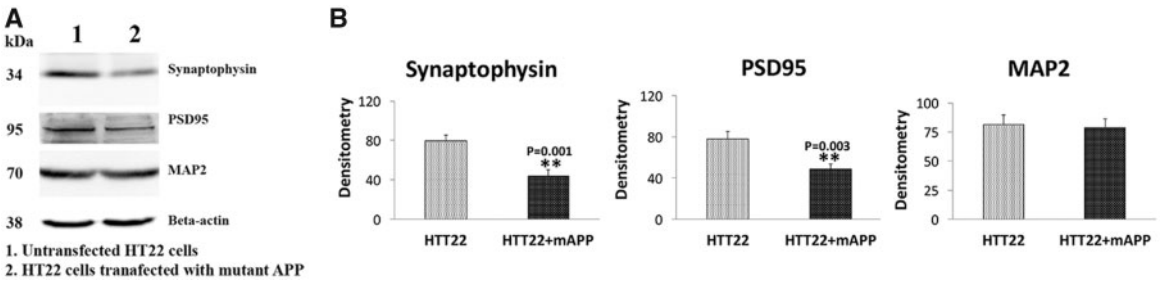

Figure 3. Immunoblotting analysis of synaptic and dendritic protein MAP2 in mutant APP-HT22 cells. Figure 3A shows representative immunoblotting analysis of HT22 cells transfected and untransfected with mutant APP cDNA. Figure 3B shows quantitative densitometry analysis of synaptic and MAP2 proteins. Synaptophysin ($P=0.001$) and PSD 95 ($P=0.003$) were significantly decreased in HT22 cells transfected with mutant APP cDNA relative to untransfected HT22 cells.

mAPP-HT22 cells, but not in untransfected, WT-HT22 cells, indicating that mAPP transfection was successful.

Mitochondrial dynamics proteins

Significantly increased levels of fission proteins Drp1 ($P = 0.003$) and Fis1 ($P = 0.01$) were found in mAPP-HT22 cells relative to untransfected, WT-HT22 cells. On the contrary, mitochondrial fusion proteins Mfn1 ($P = 0.002$), Mfn2 ($P = 0.03$) and Opa1 ($P = 0.01$) were significantly decreased, in mAPP-HT cells relative to WT-HT22 cells (Fig. 2A and B).

Mitochondrial biogenesis

As shown in Figure 2A and B, significantly decreased levels of biogenesis proteins, PGC1α ($P = 0.001$), NRF1 ($P = 0.01$), NRF2 ($P = 0.02$) and TFAM ($P = 0.01$) were found in mAPP-HT22 cells relative to untransfected, WT-HT22 cells, indicating that mitochondrial biogenesis was reduced in mAPP-HT22 cells.

Dendritic and synaptic proteins

Significantly decreased level of MAP2 ($P = 0.04$) and synaptic proteins synaptophysin ($P = 0.03$) and PSD95 ($P = 0.04$) were found in mAPP-HT cells relative to untransfected, WT-HT22 cells (Fig. 3A and B).

Autophagy proteins

Significantly decreased levels of mitophagy/autophagy proteins, PINK1 ($P = 0.001$), ATG5 ($P = 0.01$), LC3BI ($P = 0.02$), LC3BII ($P = 0.02$) and TERT ($P = 0.01$) were found in mAPP-HT22 cells relative to untransfected WT-HT22 cells, indicating that autophagy was defective in mAPP-HT22 cells (Fig. 4A and B).

Immunofluorescence analysis

Using immunofluorescence analysis, localizations and levels of MAP2, we assessed in MAP2 immunoreactivity in mAPP-HT22 cells and WT-HT22 cells.

Mitochondrial fission and fusion proteins

To determine the effect of mAPP and Aβ on protein levels and localizations, we performed immunofluorescence analysis of mitochondrial fission proteins (Drp1 and Fis1), fusion proteins (Mfn1, Mfn2 and Opa1) on mAPP-HT22 cells and untransfected,

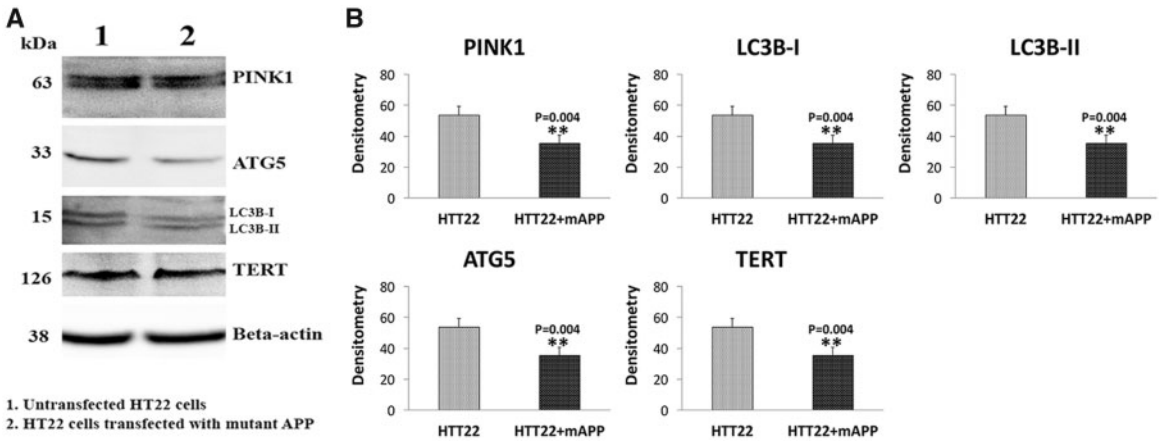

Figure 4. Immunoblotting analysis of autophagy and mitophagy proteins in mutant APP-HT22 cells. Figure 4A shows representative immunoblotting analysis of HT22 cells transfected and untransfected with mutant APP cDNA. Figure 4B shows quantitative densitometry analysis of autophagy proteins. Autophagy proteins ATG5 (P=0.004), LC3BI (P=0.004), LC3BII (P=0.004) and TERT (P=0.004) and mitophagy protein PINK (P=0.04) were significantly decreased in HT22 cells transfected with mutant APP cDNA relative to untransfected HT22 cells.

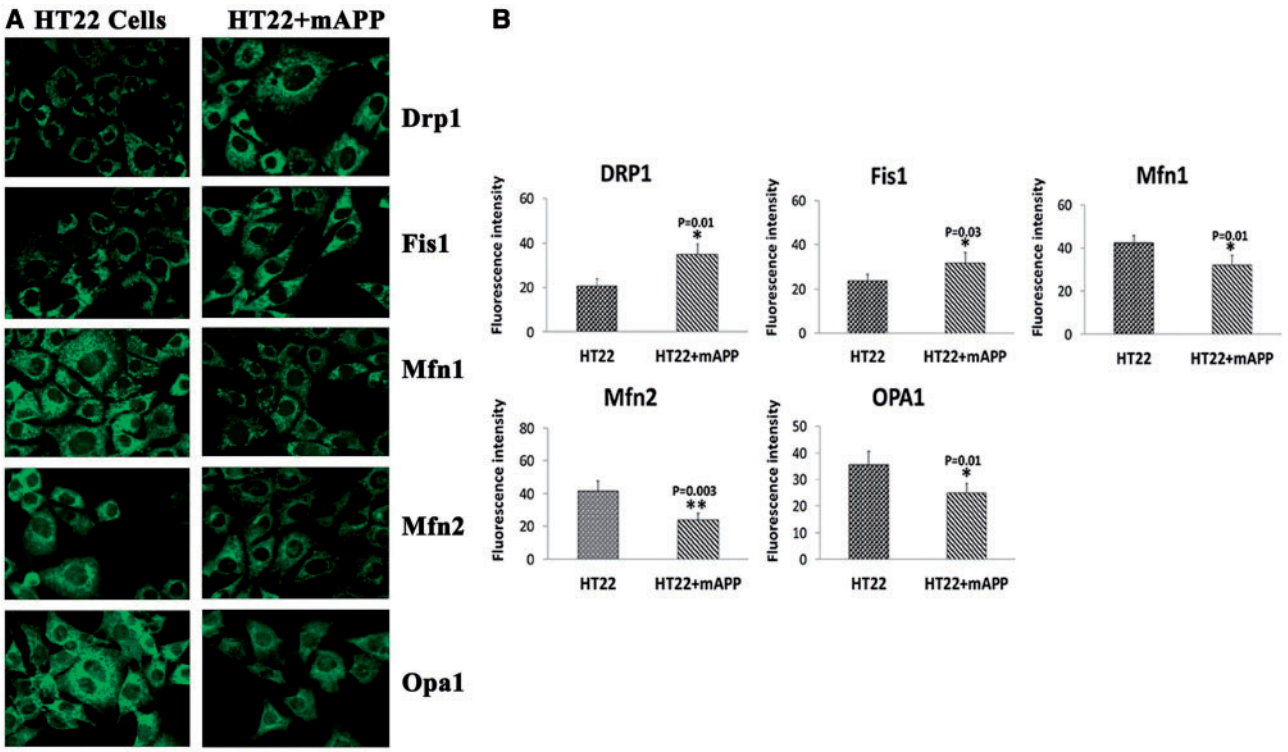

Figure 5. Immunofluorescence analysis of mitochondrial dynamics proteins in HT22 cells transfected with mutant APP cDNA relative to untransfected HT22 cells. Figure 5A presents representative images of immunofluorescence analysis. Figure 5B represents quantitative immunofluorescence analysis. Significantly increased levels of Drp1 (P=0.01), Fis1 (P=0.03) and significantly decreased levels of Mfn1 (P=0.01), Mfn2 (P=0.003) and Opa1 (P=0.01) were found in HT22 cells transfected with mutant APP cDNA relative to untransfected HT22 cells.

WT-HT22 cells. As shown in Figure 5A and B, we found significantly increased levels of Drp1 ($P = 0.01$) and Fis1 ($P = 0.03$); and significantly decreased levels of Mfn1 ($P = 0.01$), Mfn2 ($P = 0.03$) and Opa1 ($P = 0.01$) in the mAPP-HT22 cells relative to WT-HT22 cells, indicating that mAPP and Aβ increase fission activity and reduce fusion activity in mAPP-HT22 cells.

Mitochondrial biogenesis proteins

Significantly decreased levels of PGC1∝ ($P = 0.005$), NRF1 ($P = 0.02$), NRF2 ($P = 0.01$) and TFAM ($P = 0.003$) in mAPP-HT22 cells relative to untransfected, WT-HT22 cells, indicating that mAPP and Aβ decrease hippocampal mitochondrial biogenesis activity (Fig. 6A and B).

Synaptic proteins

To determine the toxic effects of mAPP and Aβ on hippocampal cells, we performed immunofluorescence analysis using synaptophysin and PSD95 antibodies. As shown in Figure 7A and B, synaptophysin ($P = 0.002$) and PSD95 ($P = 0.001$) were

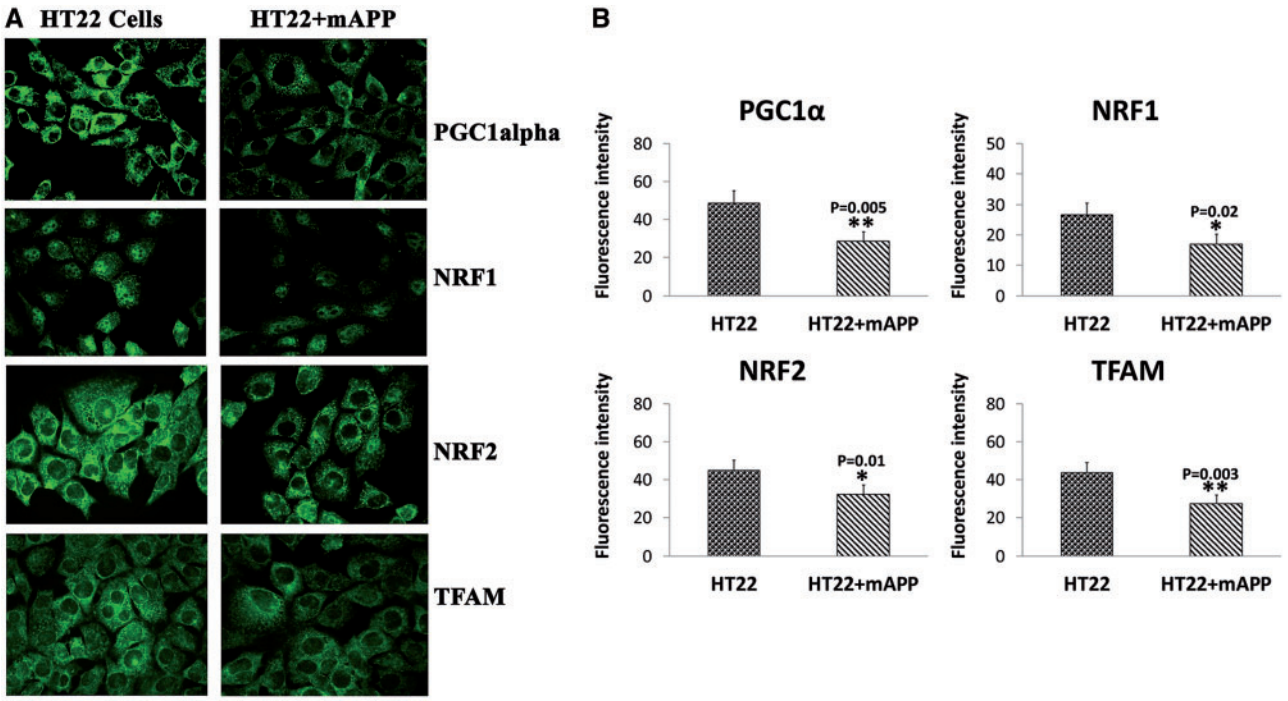

Figure 6. Immunofluorescence analysis of mitochondrial biogenesis proteins in HT22 cells transfected with mutant APP cDNA relative to untransfected HT22 cells. Figure 6A representative images of immunofluorescence analysis. Figure 6F presents representative quantitative immunofluorescence analysis. Significantly decreased levels of PGC1α (P=0.005), NRF1 (P=0.02), NRF2 (P=0.01) and TFAM (P=0.003) in HT22 cells transfected with mutant APP cDNA relative to untransfected HT22 cells.

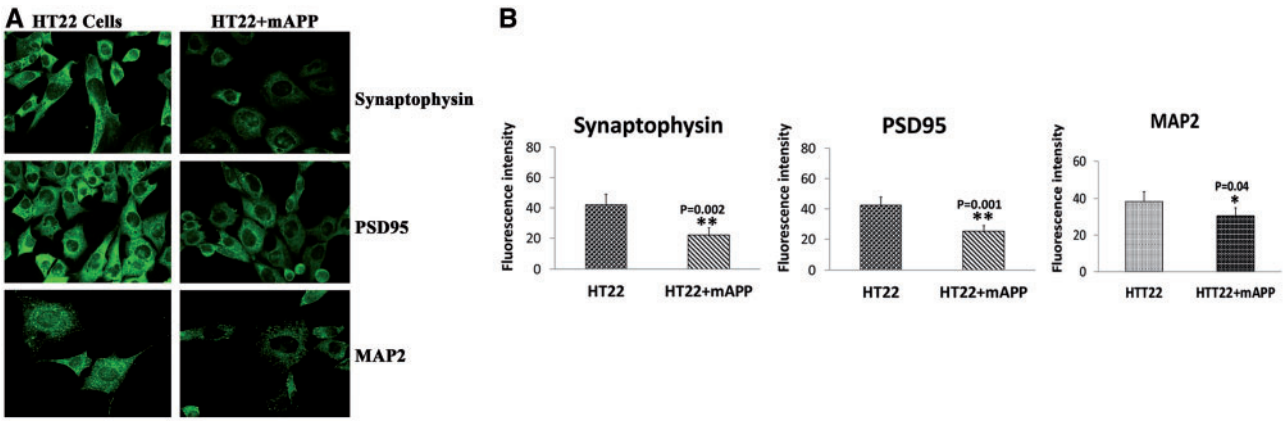

Figure 7. Immunofluorescence analysis of synaptic and dendritic proteins in HT22 cells transfected with mutant APP cDNA relative to untransfected HT22 cells. Figure 7A presents representative images of immunofluorescence analysis. Figure 7B represents quantitative immunofluorescence analysis. Significantly increased levels of synaptophysin (P=0.002), PSD95 (P=0.001) and MAP2 (P=0.04) were found in HT22 cells transfected with mutant APP cDNA relative to untransfected HT22 cells.

significantly decreased in mAPP-HT22 cells relative to untransfected, WT-HT22 cells.

Dendritic protein MAP2

As shown in Figure 7A and B, significantly decreased levels of MAP2 ($P = 0.04$) were found in mAPP-HT22 cells relative to untransfected, WT-HT22 cells, indicating that mAPP reduces MAP2 in HT22 cells.

Autophagy and mitophagy proteins

We also performed immunofluorescence analysis of autophagy ATG5, TERT, LC3B and mitophagy proteins, in mAPP-HT22 cells. As shown in Figure 8A and B, we significantly decreased levels of ATG5 ($P = 0.002$), TERT ($P = 0.01$), LC3B ($P = 0.003$) and PINK1 ($P = 0.01$) and in mAPP-HT22 cells, indicating that mAPP and Aβ affect hippocampal autophagy and mitophagy activities.

Mitochondrial function

Mitochondrial function was assessed in mAPP-HT22 cells and WT-HT22 cells by measuring H_2O_2, lipid peroxidation, cytochrome c oxidase activity and mitochondrial ATP.

H_2O_2 production

As shown in Figure 9A, significantly increased levels of H_2O_2 were found in APP-HT22 cells relative to WT-HT22 cells ($P = 0.02$), indicating that mAPP and Aβ increase H_2O_2 levels in mAPP-HT22 cells.

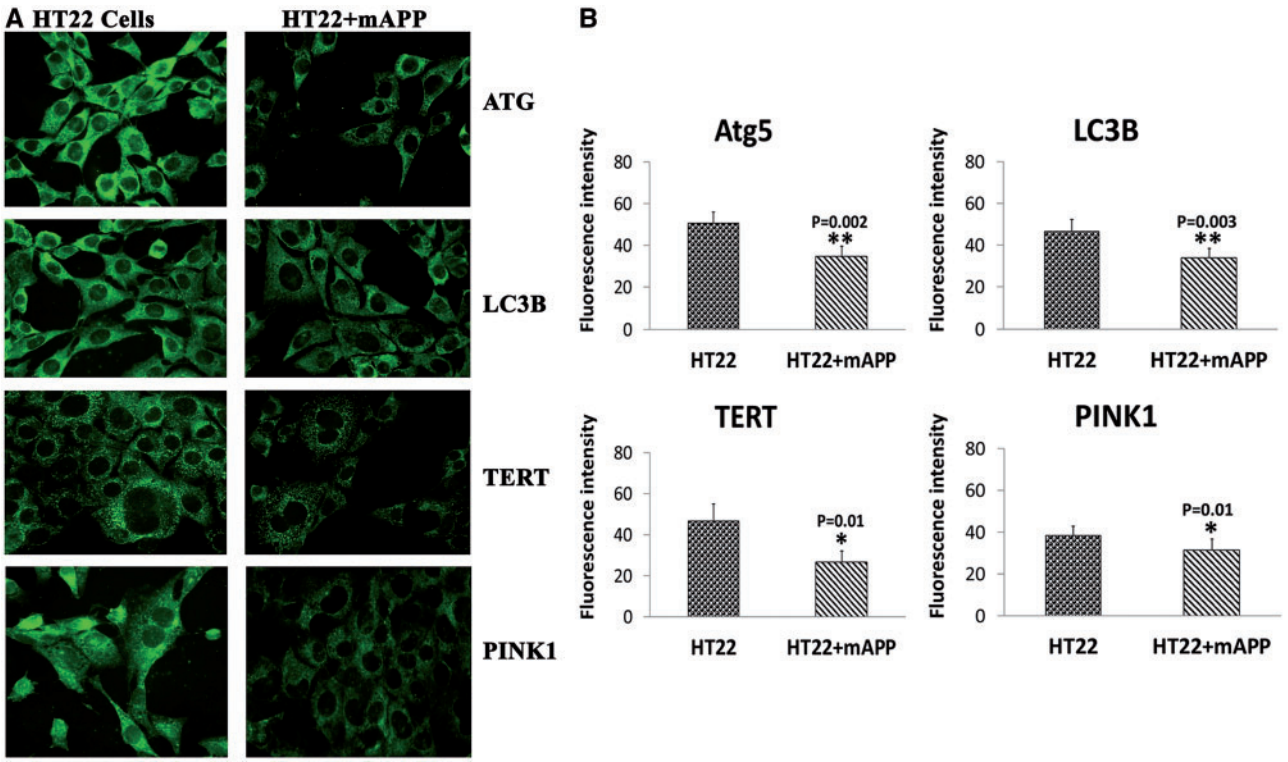

Figure 8. Immunofluorescence analysis of mitophagy and autophagy proteins in HT22 cells transfected with mutant APP cDNA relative to untransfected HT22 cells. Figure 8A, presents representative images of immunofluorescence analysis. Figure 8F represents quantitative immunofluorescence analysis. Significantly decreased levels of autophagy proteins ATG5 ($P=0.002$), LCB3 ($P=0.003$) and TERT ($P=0.01$) and mitophagy protein PINK1 ($P=0.01$) in HT22 cells transfected with mutant APP cDNA relative to untransfected HT22 cells.

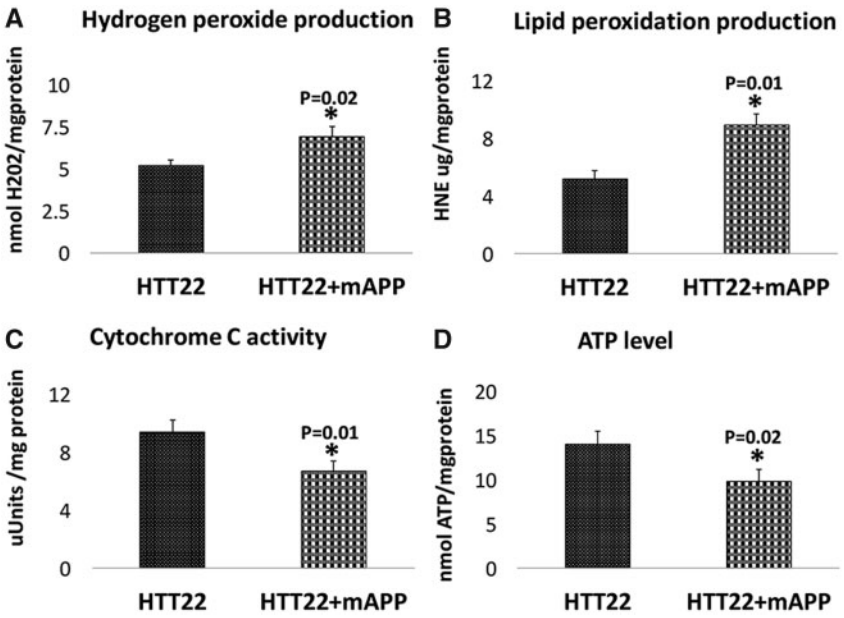

Figure 9. Mitochondrial functional parameters in in mutant APP-HT22 cells. Mitochondrial function was assessed by measuring: **(A)** H_2O_2 production, **(B)** lipid peroxidation, **(C)** cytochrome coxidase activity and **(D)** ATP levels. The levels of H_2O_2 ($P=0.02$) and 4-hydroxy-2-nonenol ($P=0.01$) were significantly increased and the levels of cytochrome coxidase ($P=0.01$) and ATP ($P=0.02$) significantly decreased found in HT22 cells transfected with mutant APP cDNA relative to untransfected HT22 cells.

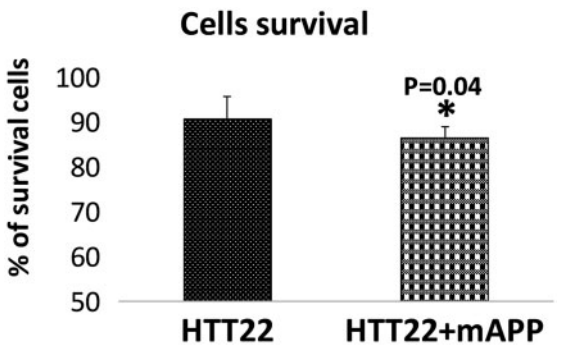

Figure 10. Cell survival percentage in mutant APP-HT22 cells. Cell survival percentage was assessed in HT22 cells transfected with mutant APP cDNA relative to untransfected HT22 cells. Significantly decreased cell survival percentage (P=0.04) was observed in HT22 cells transfected with mutant APP cDNA relative to untransfected HT22 cells.

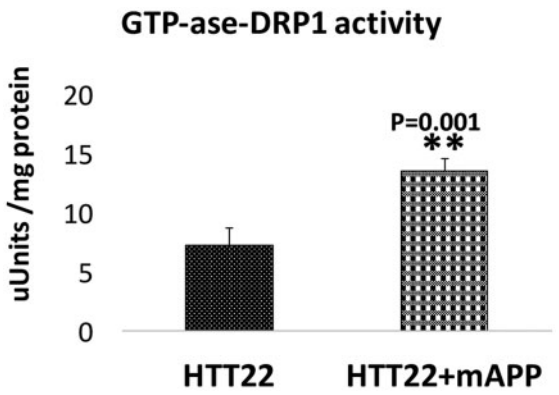

Figure 11. GTPase Drp1 enzymatic activity in mutant APP-HT22 cells. GTPase Drp1 enzymatic activity was assessed using Drp1 immunoprecipitation elutes from HT22 cells transfected with mutant APP cDNA relative to untransfected HT22 cells. Significantly increased levels of GTPase Drp1 activity levels (P=0.001) were found in HT22 cells transfected with mutant APP cDNA relative to untransfected HT22 cells.

Lipid peroxidation

Similar to H_2O_2, levels of 4-hydroxy-2-nonenol (HNE), an indicator of lipid peroxidation, were significantly increased in APP-HT22 cells (P = 0.01) relative to WT-HT22 cells (Fig. 9B).

Cytochrome c oxidase activity

Significantly decreased levels of cytochrome coxidase activity were found in mAPP-HT22 cells and relative to untransfected, WT-HT22 cells (P = 0.01), indicating that mAPP and Aβ reduce cytochrome coxidase activity (Fig. 9C).

ATP production

As shown in Figure 9D, significantly decreased levels of mitochondrial ATP were found in mAPP-HT22 cells relative to WT-HT22 cells (P = 0.02), indicating that mAPP and Aβ affect mitochondrial ATP.

Cell survival

We also assessed cell survival in mAPP-HT22 cells in order to determine the toxic effects of mAPP on cell survival. As shown in Figure 10, we found significantly decreased cell survival in mAPP-HT22 cells relative to untransfected, WT-HT22 cells (P = 0.04), indicating that mAPP is toxic and reduces cell survival of hippocampal cells.

GTPase Drp1 activity

To determine the effects of mAPP and Aβ in hippocampal cells on GTPase Drp1 activity, we assessed GTPase Drp1 activity using immunoprecipitation elutes from mAPP-HT22 cells and untransfected, WT-HT22 cells. As shown in Figure 11, we found significantly increased levels of GTPase Drp1 activity in mAPP-HT22 cells relative to untransfected WT-HT22 cells (P = 0.001), indicating that mAPP and Aβ increase GTPase activity in hippocampal cells.

Transmission electron microscopy

To determine the effects of mutant tau on mitochondrial number and length, we used transmission electron microscopy on mAPP-HT22 cells and untransfected, WT-HT22 cells.

Mitochondrial number in mutant APP-HT22 cells

As shown in Figure 12, we found significantly increased number of mitochondria in APP-HT22 cells (P = 0.005) relative to untransfected, WT-HT22 cells, suggesting that mAPP and Aβ fragment hippocampal mitochondria.

Mitochondrial length in hippocampus

We also measured mitochondrial length in order to understand whether mAPP and Aβ alter mitochondrial length. As shown in Figure 12, we found mitochondrial length is significantly decreased in APP-HT22 cells (P = 0.01) relative to untransfected-WT-HT22 cells.

Discussion

The purpose of our study was to critically assess the toxic effects of mAPP and Aβ in mouse primary hippocampal neurons transfected with mAPP cDNA that express Swedish and Indiana mutations. Using molecular, biochemical, cytochemistry, transmission electron microscopy—we studied mRNA and protein levels of mitochondrial dynamics, biogenesis, synaptic, dendritic, autophagy/mitophagy genes, and assessed GTPase Drp1 enzymatic activity, cell survival in mAPP-HT22 cells and untransfected, WT-HT22 cells. Mitochondrial function was assessed by measuring the levels of H_2O_2, lipid peroxidation, cytochrome c oxidase activity and mitochondrial ATP. Using transmission electron microscopy, we assessed mitochondrial number and length.

Increased levels of mitochondrial fission and decreased levels of fusion, biogenesis, autophagy/mitophagy, synaptic, dendritic proteins were found in mAPP-HT22 cells relative to untransfected WT-HT22 cells, indicating that the presence of abnormal mitochondrial dynamics and biogenesis, and defective synaptic, autophagy/mitophagy and dendritic activities in mAPP-HT22 cells. Mitochondrial dysfunction was defective. Transmission electron microscopy revealed significantly increased mitochondrial numbers and reduced mitochondrial length in mAPP-HT22 cells. These findings suggest that mAPP and Aβ are responsible for reduced dendritic protein MAP2, synaptic, autophagy/mitophagy and mitochondrial fusion and biogenesis proteins in mAPP-HT22 cells.

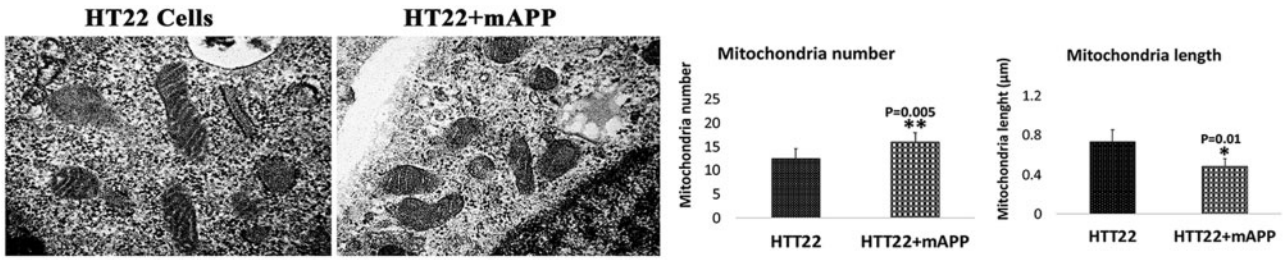

Figure 12. Mitochondrial number and length in mutant APP-HT22 cells. Figure 12A presents representative transmission electron microscopy images of mitochondria in HT22 cells transfected with mutant APP cDNA relative to untransfected HT22 cells. Figure 12B represents mitochondrial number and length in HT22 cells transfected with mutant APP cDNA relative to untransfected HT22 cells. Significantly increased number of mitochondria were found in HT22 cells transfected with mutant APP cDNA (P=0.005) relative to untransfected HT22 cells, suggesting that Aβ fragments hippocampal mitochondria. On the contrary, mitochondrial length is significantly decreased in HT22 cells transfected with mutant APP cDNA (P=0.01) relative to untransfected HT22 cells.

Hippocampal mutant APP and Aβ-induced abnormal mitochondrial changes

Impaired mitochondrial dynamics

In this study, we found increased mRNA and protein levels of mitochondrial fission genes and reduced fusion genes in hippocampal cells that express mAPP and Aβ and these observations concur with earlier studies of hippocampal tissues from 12-month-old APP transgenic mice (19) and also mouse neuroblastoma cells incubated with Aβ peptide (20) and APP primary neuronal cultures (21). The mechanistic link for the observed impaired mitochondrial dynamics (increased fission and decreased fusion) is likely due to physical interaction between mitochondrial fission protein Drp1 and Aβ that results increased levels of GTPase Drp1 activity and ultimately excessive fragmentation of mitochondria (19–22). The novelty of our current study findings is abnormal mitochondrial dynamics occur in mAPP-hippocampal cells, further strengthen our earlier observations of Drp1–Aβ interaction and increased fission machinery in AD (19–22).

Our current study findings (reduced dendritic protein MAP2, synaptic, autophagy/mitophagy and mitochondrial fusion and biogenesis proteins, and increased mitochondrial numbers and reduced mitochondrial length) also strongly support earlier observation of mAPP and Aβ association with mitochondria, causing mitochondrial and synaptic damages in AD neurons (23–25).

Defective mitochondrial biogenesis

This study observations of reduced mRNA and protein levels of mitochondrial biogenesis genes, including PGC1α, Nrf1, Nrf2 and TFAM in mAPP hippocampal cells strongly agree with our recent study findings of hippocampal tissues from 12-month-old APP mice (19) and other studies of hippocampal tissues from mutant tau mice (26) and cortical tissues from APP mice (27) and postmortem AD brains (28). These observations indicate that reduced mitochondrial biogenesis is a typical AD feature. Enhancement of mitochondrial biogenesis is an ideal therapeutic approach in AD.

Mutant APP and Aβ-induced defective autophagy and mitophagy in hippocampal cells

In this study, we found reduced mRNA and protein levels of autophagy ATG5, LC3BI & LC3BII and mitophagy proteins PINK1 and TERT in hippocampal cells that express mAPP and Aβ, indicating that abnormal accumulation of mAPP and Aβ affects autophagy and mitophagy in hippocampal cells, these observations agree with our recent findings of hippocampal tissues from 12-month-old APP mice (19) and other APP mice studies (29). These findings indicate that defective autophagy and mitophagy are AD characteristic features. Further, our observations of defective autophagy and mitophagy in mAPP-HT22 cells strongly agree with mammalian target of rapamycin (mTOR) involvement of mAPP and Aβ with autophagy and mitophagy in AD (30,31). Based on these observations, we propose that enhancing and/or correcting autophagy and mitophagy activities are possible therapeutic approaches for AD.

Hippocampal mutant APP and Aβ-induced reduced synaptic and dendritic proteins

Increasing evidence suggests that spine density is critical for synaptic and cognitive functions in AD patients and AD mice. In this study, we assessed mAPP and Aβ and synaptic and dendritic proteins in mAPP-HT22 cells. We found increased full-length APP in mAPP hippocampal cells, but not in WT-HT22 cells. Significantly reduced levels of pre-synaptic protein, synaptophysin and postsynaptic density protein, PSD95 in mAPP-HT22 cells and reduced dendritic protein mAP2. These changes in mAPP hippocampal cells, including increased full-length mAPP and reduced dendritic protein MAP2, reduced synaptic proteins are undoubtedly responsible for synaptic damage and cognitive functions in AD.

Mitochondrial structural and functional changes

In this study, mitochondrial function was defective mAPP-HT22 cells. Our current study observations of increased lipid peroxidation and H_2O_2 levels and reduced cytochrome c oxidase activity and mitochondrial ATP in mAPP hippocampal cells agree with results of hippocampal tissues from 12-month-old APP mice (19). These observations further confirm that defective mitochondrial function is mainly due to mAPP and Aβ-induced impaired mitochondrial dynamics and biogenesis in hippocampal cells. Further, it is possible that accumulation of mAPP and Aβ in hippocampal cells is responsible for synaptic toxicities—reduced synaptophysin and PSD95 in hippocampal cells.

Our current study findings of mitochondrial structural changes in mAPP hippocampal cells—increased mitochondrial number and reduced mitochondrial length further strengthen our hypothesis that mAPP and Aβ induce mitochondrial abnormalities, including changes in increased mitochondrial number and reduced mitochondrial length and mitochondrial dysfunction in hippocampal cells in AD. These observations agreed with our lab publication of hippocampal tissues12-month-old APP mice (19).

In summary, mAPP and Aβ increase mitochondrial fragmentation, reduce fission, biogenesis, synaptic activity and also

reduce mitophagy and autophagy activities in hippocampal cells. Further, novelty studying primary hippocampal neurons (HT22) is that these cells can be used for drug screening using high throughput machines and tools. As described in this study, primary mouse hippocampal neurons after transfection with mAPP cDNA mimic similar features of transgenic APP mice. Unlike transgenic APP mice, primary hippocampal neurons are quick to test drugs for Aβ pathology, changes in mitophagy and autophagy, mitochondrial and synapses. Overall, mAPP-HT22 cells are good candidates for high throughput drug screening for AD.

Materials and Methods

Chemicals and reagents

HT22 cells were a kind gift from David Schupert, Dulbecco's modified Eagle medium (DMEM) and minimum essential medium (MEM), penicillin/streptomycin, Trypsin-EDTA, and fetal bovine serum were purchased from GIBCO (Gaithersberg, MD, USA).

Mutant APP cDNA construct

We purchased mutant APP Swe cDNA clone (pCAX-APP Swe/Ind) from Addgene—https://www.addgene.org and further subcloned into a mammalian expression vector pRP-Puro-CAG. pRP vector is pUC backbone having CMV promoter and SV40 polyadenylation site with puromycin selection for stable transfection. The sequence output was confirmed with NCBI sequence hAPP [NM_201414.2]*(K595N M596L V642F). Expression of mutant APP APP Swe/Ind cDNA was verified for APP mutant protein expression. We transfected mutant APP Swe/Ind cDNA into HT cells using lipofectamine 3000 for 24 h. After transfection, cells were harvested and pellet was used for RNA and protein analysis.

Tissue culture work

The HT22 cells were grown for 3 days in a medium [1:1 mixture of DMEM and OptiMEM, 10% FBS plus penicillin and streptomycin (Invitrogen, Carlsbad, CA, USA)] until the cells are confluent. We performed four independent cell cultures and transfections with mAPP cDNA treatments for all experiments ($n = 4$).

Mitochondrial functional assays by measuring H_2O_2, lipid peroxidation, cytochrome c oxidase activity, and MTT determination, and apoptosis assay. We also assessed GTPase Drp1 enzymatic activity. Amyloid beta (Aβ) levels were measured using sandwich ELISA assay. Mitochondrial ATP was measured from isolated mitochondria in cells.

Quantification of mRNA expression of mitochondrial dynamics, mitochondrial biogenesis and synaptic genes using real-time RT-PCR

Using the reagent TriZol (Invitrogen), we isolated total RNA from mAPP-HT22 cells and untransfected WT-HT22 cells. Using primer express Software (Applied Biosystems), we designed the oligonucleotide primers for the housekeeping genes β-actin; glyceraldehyde 3-phosphate dehydrogenase (GAPDH); mitochondrial biogenesis genes PGC1α, Nrf1, Nrf2 and TFAM, mitochondrial structural genes; fission (Drp1 and Fis1); fusion genes (MFN1, MFN2, Opa1) and autophagy (ATG5 & LC3BI, LC3BII), mitophagy (PINK1 & TERT, BCL2 & BNIPBL) and synaptic genes (synaptophysin and PSD95). The primer sequences and amplicon sizes are listed in Table 2. With SYBR-Green chemistry-based quantitative real-time RT-PCR, we measured mRNA expression of the genes mentioned above as described by Manczak et al. (2011) (22). Briefly, 2 μg of DNAse-treated total RNA was used as starting material, to which we added 1 μl of oligo (dT), 1 μl of 10 mM dNTPs, 4 μl of 5× first strand buffer, 2 μl of 0.1 M DTT, and 1 μl RNAse outout. The reagents RNA, dT and dNTPs were mixed first, then heated at 65°C for 5 min, and finally chilled on ice until the remaining components were added. The samples were incubated at 42°C for 2 min, and then 1 μl of Superscript III (40 U/μl) was added. The samples were then incubated at 42°C for 50 min, at which time the reaction was inactivated by heating at 70°C for 15 min.

Quantitative real-time PCR amplification reactions were performed in an ABI Prism 7900 sequence detection system (Applied Biosystems, Foster City, CA) in a 25 μl volume of total reaction mixture as described in Reddy *et al.* (2016) (32). All RT-PCR reactions were carried out in triplicate, with no template control. The PCR conditions were: 50°C for 2 min and 95°C for 10 min, followed by 40 cycles of 95°C for 15 s and 60°C for 1 min. The fluorescent spectra were recorded during the elongation phase of each PCR cycle. To distinguish specific amplicons from non-specific amplifications, a dissociation curve was generated. The CT-values were calculated with sequence-detection system (SDS) software V1.7 (Applied Biosystems) and an automatic setting of base line, which was the average value of PCR, cycles 3–15, plus CT generated 10 times its standard deviation. The amplification plots and CT-values were exported from the exponential phase of PCR directly into a Microsoft Excel worksheet for further analysis.

The mRNA transcript level was normalized against β-actin and the GAPDH at each dilution. The standard curve was the normalized mRNA transcript level, plotted against the log-value of the input cDNA concentration at each dilution. To compare β-actin, GAPDH and genes of interest shown in Table 2, relative quantification was performed according to the CT method (Applied Biosystems). Briefly, the comparative CT method involved averaging triplicate samples, which were taken as the CT values for β-actin, GAPDH and genes of interest. β-actin normalization was used in this study because β-actin CT values were similar for the control untreated cells and experimental groups. The ΔCT-value was obtained by subtracting the average β-actin CT value from the average CT-value of for the genes of interest. The ΔCT of WT-HT22 cells was used as the calibrator. The fold change was calculated according to the formula $2-(\Delta\ \Delta CT)$, where ΔΔCT is the difference between ΔCT and the ΔCT calibrator value. Statistical significance was calculated (1) between mRNA expression in mAPP-HT22 cells and untransfected WT-HT22 cells using the CT value difference.

Immunoblotting analysis

Immunoblotting analysis was performed using protein lysates prepared HT-22 cells transfected and untransfected mAPP cDNA using 6E10 antibody that recognizes full-length mutant human APP and Aβ as described in Manczak *et al.* (2010) (20). We also performed immunoblotting analysis for mitochondrial dynamics, biogenesis, synaptic, autophagy and mitophagy proteins. Details of antibody dilutions are given in Table 3. Protein lysates (20 μg) were resolved on a 4–12% Nu-PAGE gel (Invitrogen). The resolved proteins were transferred to nylon membranes (Novax Inc., San Diego, CA, USA) and were then

Table 2. Summary of qRT-PCR oligonucleotide primers used in measuring mRNA expressions in mitochondrial dynamics and mitochondrial biogenesis, synaptic, autophagy and mitophagy genes in mAPP-HT22 cells compared to untransfected WT-HT22 cells

Gene	DNA sequence (5′-3′)	PCR product size
	Mitochondrial dynamics genes	
Drp1	Forward primer ATGCCAGCAAGTCCACAGAA	86
	Reverse primer TGTTCTCGGGCAGACAGTTT	
Fis1	Forward primer CAAAGAGGAACAGCGGGACT	95
	Reverse primer ACAGCCCTCGCACATACTTT	
Mfn1	Forward primer GCAGACAGCACATGGAGAGA	83
	Reverse primer GATCCGATTCCGAGCTTCCG	
Mfn2	Forward primer TGCACCGCCATATAGAGGAAG	78
	Reverse primer TCTGCAGTGAACTGGCAATG	
Opa1	Forward primer ACCTTGCCAGTTTAGCTCCC	82
	Reverse primer TTGGGACCTGCAGTGAAGAA	
	Mitochondrial biogenesis genes	
PGC1α	Forward primer GCAGTCGCAACATGCTCAAG	83
	Reverse primer GGGAACCCTTGGGGTCATTT	
Nrf1	Forward primer AGAAACGGAAACGGCCTCAT	96
	Reverse primer CATCCAACGTGGCTCTGAGT	
Nrf2	Forward primer ATGGAGCAAGTTTGGCAGGA	96
	Reverse primer GCTGGGAACAGCGGTAGTAT	
TFAM	Forward primer TCCACAGAACAGCTACCCAA	84
	Reverse primer CCACAGGGCTGCAATTTTCC	
	Reverse primer AGACGGTTGTTGATTAGGCGT	
	Synaptic genes	
Synaptophysin	Forward primer CTGCGTTAAAGGGGGCACTA	81
	Reverse primer ACAGCCACGGTGACAAAGAA	
PSD95	Forward primer CTTCATCCTTGCTGGGGGTC	90
	Reverse primer TTGCGGAGGTCAACACCATT	
	Autophagy genes	
LC3A	Forward primer CCCATCGCTGACATCTATGAAC	77
	Reverse primer AAGGTTTCTTGGGAGGCGTA	
LC3B	Forward primer TCCACTCCCATCTCCGAAGT	94
	Reverse primer TTGCTGTCCCGAATGTCTCC	
ATG5	Forward primer TCCATCCAAGGATGCGGTTG	95
	Reverse primer TCTGCATTTCGTTGATCACTTGAC	
Beclin1	Forward primer ACCAGCGGGAGTATAGTGAGT	98
	Reverse primer CAGCTGGATCTGGGCGTAG	
	Mitophagy genes	
Pink1	Forward primer CCATCGGGATCTCAAGTCCG	70
	Reverse primer GATCACTAGCCAGGGACAGC	
TERT	Forward primer GCAAGGTGGTGTCTGCTAGT	100
	Reverse primer AGCTTGCCGTATTTCCCCAA	
BCL2	Forward primer TCCTTCCAGCCTGAGAGCAA	73
	Reverse primer GCCTGAGAGGAGACGTCCTG	
BNIP3L	Forward primer GCACGTTCCTTCCTCGTCT	82
	Reverse primer GCTCTGTCCCGACTCATGC	
	Housekeeping genes	
B-actin	Forward primer AGAAGCTGTGCTATGTTGCTCTA	91
	Reverse primer TCAGGCAGCTCATAGCTCTTC	
GAPDH	Forward primer TTCCCGTTCAGCTCTGGG	59
	Reverse primer CCCTGCATCCACTGGTGC	

incubated for 1 h at room temperature with a blocking buffer (5% dry milk dissolved in a TBST buffer). The nylon membranes were incubated overnight with the primary antibodies. The membranes were washed with a TBST buffer three times at 10 min intervals and were then incubated for 2 h with appropriate secondary antibody Sheep anti-mouse HRP 1:10 000, followed by three additional washes at 10 min intervals. Proteins were detected with chemilumniscence reagents (Pierce Biotechnology, Rockford, IL, USA), and the bands from immunoblots were visualized.

Immunofluorescence analysis and quantification

To determine immunoreactivities of mitochondrial dynamics, biogenesis, synaptic and autophagy/mitophagy proteins, immunofluorescence analysis was performed using mAPP-HT22 cells

Table 3. Summary of antibody dilutions and conditions used in the immunoblotting analysis of mitochondrial dynamics, mitochondrial biogenesis, synaptic, autophagy and mitophagy proteins in mAPP-HT22 cells and untransfected WT-HT22 cells

Marker	Primary antibody—species and dilution	Purchased from company, city and state	Secondary antibody, dilution	Purchased from company, city and state
Drp1	Rabbit polyclonal 1:500	Novus Biological, Littleton, CO	Donkey anti-rabbit HRP 1:10 000	GE Healthcare Amersham, Piscataway, NJ
Fis1	Rabbit polyclonal 1:500	Protein Tech Group, Inc, Chicago, IL	Donkey anti-rabbit HRP 1:10 000	GE Healthcare Amersham, Piscataway, NJ
Mfn1	Rabbit polyclonal 1:400	Abcam, Cambridge, MA	Donkey anti-rabbit HRP 1:10 000	GE Healthcare Amersham, Piscataway, NJ
Mfn2	Rabbit polyclonal 1:400	Abcam, Cambridge, MA	Donkey anti-rabbit HRP 1:10 000	GE Healthcare Amersham, Piscataway, NJ
SYN	Rabbit monoclonal 1:400	Abcam, Cambridge, MA	Donkey anti-rabbit HRP 1:10 000	GE Healthcare Amersham, Piscataway, NJ
PSD95	Rabbit monoclonal 1:300	Abcam, Cambridge, MA	Donkey anti-rabbit HRP 1:10 000	GE Healthcare Amersham, Piscataway, NJ
PGC1α	Rabbit polyclonal 1:500	Novus Biological, Littleton, CO	Donkey anti-rabbit HRP 1:10 000	GE Healthcare Amersham, Piscataway, NJ
NRF1	Rabbit polyclonal 1:300	Novus Biological, Littleton, CO	Donkey anti-rabbit HRP 1:10 000	GE Healthcare Amersham, Piscataway, NJ
NRF2	Rabbit polyclonal 1:300	Novus Biological, Littleton, CO	Donkey anti-rabbit HRP 1:10 000	GE Healthcare Amersham, Piscataway, NJ
TFAM	Rabbit polyclonal 1:300	Novus Biological, Littleton, CO	Donkey anti-rabbit HRP 1:10 000	GE Healthcare Amersham, Piscataway, NJ
LC3B	Rabbit polyclonal 1:400	Novus Biological, Littleton, CO	Donkey anti-rabbit HRP 1:10 000	GE Healthcare Amersham, Piscataway, NJ
ATG5	Rabbit polyclonal 1:400	Novus Biological, Littleton, CO	Donkey anti-rabbit HRP 1:10 000	GE Healthcare Amersham, Piscataway, NJ
PINK1	Rabbit polyclonal 1:300	Novus Biological, Littleton, CO	Donkey anti-rabbit HRP 1:10 000	GE Healthcare Amersham, Piscataway, NJ
TERT	Rabbit polyclonal 1:500	Novus Biological, Littleton, CO	Donkey anti-rabbit HRP 1:10 000	GE Healthcare Amersham, Piscataway, NJ
MAP2	Mouse monoclonal 1:600	Santa Cruz Biotechnology, Dallas, TX	Sheep anti-mouse HRP 1:10 000	GE Healthcare Amersham, Piscataway, NJ
B-actin	Mouse monoclonal 1:500	Sigma-Aldrich, St Luis, MO	Sheep anti-mouse HRP 1:10 000	GE Healthcare Amersham, Piscataway, NJ

and untransfected HT22 cells and mitochondrial dynamics, biogenesis, synaptic and autophagy/mitophagy proteins as described in Manczak *et al.* (2010) (20). Details of antibody dilutions are given in Table 4. The fixed cells were washed with warm phosphate buffered saline (PBS), fixed in freshly prepared 4% paraformaldehyde in PBS for 10 min, and then washed with PBS and permeabilized with 0.1% Triton-X100 in PBS. They were blocked with a 1% blocking solution (Invitrogen) for 1 h at room temperature. All sections were incubated overnight with antibodies and dilutions described in Table 3. After incubation, the cells were washed three times with PBS, for 10 min each. The cells were incubated with a secondary antibody conjugated with Fluor 488 (Invitrogen) for 1 h at room temperature. The cells were washed three times with PBS and mounted on slides. Photographs were taken with a multiphoton laser scanning microscope system (ZeissMeta LSM510). To quantify the immunoreactivities of antibodies, 10–15 photographs were taken at ×40 magnifications and statistical significance was assessed.

Cell survival assay

Cell based apoptosis assay was performed using Cellometer Vision CBA Image Cytometry System (Nexcelom Bioscience LLC, Lawrence, MA) with two fluorophore Annexin V-FITC and propidium iodide (PI) staining solution, according to manufacturer's instructions. Briefly, cells were harvested using trypsin, then spin down at 300 g for 3 min and pellets were washed with 1XPBS, cells were counted using hematocytometer. Collected 100 000–150 000 cells and cells/pellet were re-suspended in 40 μl of Annexin V binding buffer and 5 μl each of Annexin V–FITC reagent (green) and PI (red) were added to binding buffer containing cells; gently mix solution by pipetting up and down 10 times, then incubate for 15 min at RT in the dark; after incubation, add 250 μl of 1XPBS and spin down at 300 g for 3 min, then re-suspended the cell pellets in 50 μl of Annexin V binding buffer, then assess the cells apoptosis. Gate purple represents live cells, gate green represents the positive apoptotic cells, gate blue represents for the detection of positive necrotic cells and gate red represents debris.

Measurement of soluble Aβ levels

Soluble Aβ levels were conducted using sandwich ELISA as described in Manczak *et al.* (2016) (33). Briefly, protein lysates were from cell pellets in a Tris-buffered saline (pH 8.0) containing protease inhibitors (20 mg/ml pepstatin A, aprotinin, phophsoramidon and leupeptin; 0.5 mM phenylmethanesulfonyl fluoride and 1 mM ethyleneglycol-bis(flaminoethyl ether)-NN tetraacetic acid). Samples were sonicated briefly and centrifuged at 10 000 g for 20 min at 4°C. The soluble fraction was used to determine the soluble Aβ by ELISA. For each sample, Aβ1–40 and Aβ1–42 were measured with commercial colorimetric ELISA kits (Biosource International, Camarillo, CA, USA) specific for human. A 96-well plate was used, following the manufacturer's instructions. Each sample was run in duplicate. Protein concentrations of the homogenates were determined following the BSA method, and Aβ was expressed as pg Aβ/mg protein.

Mitochondrial functional assays

Mitochondrial function was assessed by measuring H_2O_2, lipid peroxidation, cytochrome c oxidase activity and ATP in HT22 cells transfected with mAPP cDNA.

Table 4. Summary of antibody dilutions and conditions used in immunofluorescence analysis of mitochondrial dynamics, mitochondrial biogenesis, synaptic, autophagy and mitophagy proteins in mAPP-HT22 cells and untransfected WT-HT22 cells

Marker	Primary antibody—species and dilution	Purchased from company, state	Secondary antibody, dilution, Alexa Fluor dye	Purchased from company, city and state
Drp1	Rabbit polyclonal 1:200	Novus Biological, Littleton, CO	Donkey anti-rabbit IgG Alexa Fluor 488	Thermo Fisher Scientific, Waltham, MA
Fis1	Rabbit polyclonal 1:200	Protein Tech Group, Inc, Chicago, IL	Donkey anti-rabbit IgG Alexa Fluor 488	Thermo Fisher Scientific, Waltham, MA
Mfn1	Rabbit polyclonal 1:200	Protein Tech Group, Inc, Chicago, IL	Donkey anti-rabbit IgG Alexa Fluor 488	Thermo Fisher Scientific, Waltham, MA
Mfn2	Rabbit polyclonal 1:200	Protein Tech Group, Inc, Chicago, IL	Donkey anti-rabbit IgG Alexa Fluor 488	Thermo Fisher Scientific, Waltham, MA
OPA1	Rabbit polyclonal 1:300	Novus Biological, Littleton, CO	Donkey anti-rabbit IgG Alexa Fluor 488	Thermo Fisher Scientific, Waltham, MA
SYN	Rabbit polyclonal 1:400	Protein Tech Group, Inc, Chicago, IL	Donkey anti-rabbit IgG Alexa Fluor 488	Thermo Fisher Scientific, Waltham, MA
PSD95	Rabbit polyclonal 1:400	Protein Tech Group, Inc, Chicago, IL	Donkey anti-rabbit IgG Alexa Fluor 488	Thermo Fisher Scientific, Waltham, MA
PGC1α	Rabbit polyclonal 1:200	Novus Biological, Littleton, CO	Donkey anti-rabbit IgG Alexa Fluor 488	Thermo Fisher Scientific, Waltham, MA
NRF1	Rabbit polyclonal 1:300	Novus Biological, Littleton, CO	Donkey anti-rabbit IgG Alexa Fluor 48	Thermo Fisher Scientific, Waltham, MA
NRF2	Rabbit polyclonal 1:300	Novus Biological, Littleton, CO	Donkey anti-rabbit IgG Alexa Fluor 488	Thermo Fisher Scientific, Waltham, MA
TFAM	Rabbit polyclonal 1:300	Novus Biological, Littleton, CO	Donkey anti-rabbit IgG Alexa Fluor 488	Thermo Fisher Scientific, Waltham, MA
LC3B	Rabbit polyclonal 1:200	Novus Biological, Littleton, CO	Donkey anti-rabbit IgG Alexa Fluor 488	Thermo Fisher Scientific, Waltham, MA
ATG5	Rabbit polyclonal 1:200	Novus Biological, Littleton, CO	Donkey anti-rabbit IgG Alexa Fluor 488	Thermo Fisher Scientific, Waltham, MA
PINK1	Rabbit polyclonal 1:200	Novus Biological, Littleton, CO	Donkey anti-rabbit IgG Alexa Fluor 488	Thermo Fisher Scientific, Waltham, MA
TERT	Rabbit polyclonal 1:200	Novus Biological, Littleton, CO	Donkey anti-rabbit IgG Alexa Fluor 488	Thermo Fisher Scientific, Waltham, MA
MAP2	Mouse monoclonal 1:400	Santa Cruz Biotechnology, Dallas, TX	Donkey anti-mouse IgG Alexa Fluor 488	Thermo Fisher Scientific, Waltham, MA

H_2O_2 production

Using an Amplex® Red H_2O_2 Assay Kit (Molecular Probes, Eugene, OR, USA), the production of H_2O_2 was measured using cell pellets from groups of cells as described in Reddy *et al.* (2016) (32). Briefly, H_2O_2 production was measured in the mitochondria cortical tissues from all four lines of mice. A BCA Protein Assay Kit (Pierce Biotechnology) was used to estimate protein concentration. The reaction mixture contained mitochondrial proteins (μg/μl), Amplex Red reagents (50 μM), horseradish peroxidase (0.1 U/ml) and a reaction buffer (1X). The mixture was incubated at room temperature for 30 min, followed by spectrophotometer readings of fluorescence (570 nm). Finally, H_2O_2 production was determined, using a standard curve equation expressed in nmol/μg mitochondrial protein.

Lipid peroxidation assay

Lipid peroxidates are unstable indicators of oxidative stress in the brain. The final product of lipid peroxidation is HNE, which was measured in all groups of cells. We used HNE-His ELISA Kit (Cell BioLabs, Inc., San Diego, CA, USA) as described in Manczak and Reddy, 2012. Briefly, freshly prepared protein as added to a 96-well protein binding plate and incubated overnight at 4°C. It was then washed three times with a buffer. After the last wash, the anti-HNE-His antibody was added to the protein in the wells, which was then incubated for 2 h at room temperature and was washed again three times. Next, the samples were incubated with a secondary antibody conjugated with peroxidase for 2 h at room temperature, followed by incubation with an enzyme substrate. Optical density was measured (at 450 nm) to quantify the level of HNE.

Cytochrome c oxidase activity

Cytochrome c oxidase activity was measured in all groups of cells. Enzyme activity was assayed spectrophotometrically using a Sigma Kit (Sigma–Aldrich) following manufacturer's instructions. Briefly, 2 μg protein lysate was added to 1.1 ml of a reaction solution containing 50 μl 0.22 mM ferricytochrome c fully reduced by sodium hydrosulphide, Tris–HCl (pH 7.0) and 120 mM potassium chloride. The decrease in absorbance at 550 mM was recorded for 1 min reactions at 10 s intervals. Cytochrome c oxidase activity was measured according to the following formula: mU/mg total mitochondrial protein = [A/min sample − (A/min blank) × 1.1 mg protein × 21.84]. The protein concentrations were determined following the BCA method.

ATP levels

ATP levels were measured in isolated mitochondria from all groups of cells using ATP determination kit (Molecular Probes). The bioluminescence assay is based on the reaction of ATP with recombinant firefly luciferase and its substract luciferin. Luciferase catalyzes the formation of light from ATP and luciferin. It is the emitted light that is linearly related to the ATP concentration, which is measured with a luminometer. ATP levels were measured from mitochondrial pellets using a standard curve method.

GTPase Drp1 enzymatic activity

Using a calorimetric kit (Novus Biologicals, Littleton, CO, USA), GTPase Drp1 enzymatic activity was measured in mAPP-HT22

and untransfected, WT-HT22 cells using Drp1-immunoiprecipitation elutes following GTPase assay methods described in Manczak *et al.* (2011), based on GTP hydrolyzing to GDP and to inorganic Pi. GTPase activity was measured, based on the amount of Pi that the GTP produces. By adding the ColorLock Gold (orange) substrate to the Pi generated from GTP, we assessed GTP activity, based on the inorganic complex solution (green). Colorimetric measurements (green) were read in the wavelength range of 650 nm.

Statistical considerations

Statistical analyses were conducted for mAPP-HT22 cells versus untransfected WT-HT22 cells using Student *t*-test. The parameters included mRNA and protein levels H_2O_2, cytochrome c oxidase activity, lipid peroxidation, ATP production, cell viability, GTPase Drp1 activity, cell survival, cell death and Aβ levels.

Acknowledgements

We sincerely thank Dr. David Schubert for providing HT22 cell line for our study.
Conflict of Interest statement. None declared.

Funding

Work presented in this article is supported by NIH grants AG042178, AG047812 and NS105473, and the Garrison Family Foundation, CH Foundation and Alzheimer's Association SAGA grant (to PHR). Present work is also supported by Alzheimer's Association New Investigator Research Grant 2016-NIRG-39787 and Center of Excellence for Translational Neuroscience and Therapeutics grant number PN-CTNT20115-AR and Sex and Gender Alzheimer's Association (SAGA) grant (to APR).

References

1. Selkoe, D.J. (2001) Alzheimer's disease: genes, proteins, and therapy. *Physiol. Rev.*, **81**, 741–766.
2. Reddy, A.P. and Reddy, P.H. (2017) Mitochondria-targeted molecules as potential drugs to treat patients with Alzheimer's disease. *Prog. Mol. Biol. Transl. Sci.*, **146**, 173–201.
3. World Alzheimer Report. (2016) Improving healthcare for people living with dementia: coverage, quality and costs now and in the future.
4. McGeer, P.L. and McGeer, E.G. (2001) Inflammation, autotoxicity and Alzheimer disease. *Neurobiol. Aging*, **22**, 799–809.
5. Zhu, X., Perry, G., Smith, M.A. and Wang, X. (2013) Abnormal mitochondrial dynamics in the pathogenesis of Alzheimer's disease. *J. Alzheimers Dis.*, **33 (Suppl. 1)**, S253–S262.
6. Wang, X., Su, B., Siedlak, S.L., Moreira, P.I., Fujioka, H., Wang, Y., Casadesus, G. and Zhu, X. (2008) Amyloid-beta overproduction causes abnormal mitochondrial dynamics via differential modulation of mitochondrial fission/fusion proteins. *Proc. Natl. Acad. Sci. U S A*, **105**, 19318–19323.
7. Swerdlow, R.H., Burns, J.M. and Khan, S.M. (2014) The Alzheimer's disease mitochondrial cascade hypothesis: progress and perspectives. *Biochim. Biophys. Acta*, **1842**, 1219–1231.
8. Reddy, P.H., Manczak, M., Mao, P., Calkins, M.J., Reddy, A.P. and Shirendeb, U. (2010) Amyloid-beta and mitochondria in aging and Alzheimer's disease: implications for synaptic damage and cognitive decline. *J. Alzheimers Dis.*, **20**, S499–S512.
9. Reddy, P.H., Tripathi, R., Troung, Q., Tirumala, K., Reddy, T.P., Anekonda, V., Shirendeb, U.P., Calkins, M.J., Reddy, A.P., Mao, P. and Manczak, M. (2012) Abnormal mitochondrial dynamics and synaptic degeneration as early events in Alzheimer's disease: implications to mitochondria-targeted antioxidant therapeutics. *Biochim. Biophys. Acta*, **1822**, 639–649.
10. LaFerla, F.M., Green, K.N. and Oddo, S. (2007) Intracellular amyloid-beta in Alzheimer's disease. *Nat. Rev. Neurosci.*, **8**, 499–509.
11. Braak, H. and Braak, E. (1991) Demonstration of amyloid deposits and neurofibrillary changes in whole brain sections. *Brain. Pathol.*, **1**, 213–216.
12. Hyman, B.T., Van Hoesen, G.W., Kromer, L.J. and Damasio, A.R. (1986) Perforant pathway changes and the memory impairment of Alzheimer's disease. *Ann. Neurol.*, **20**, 472–481.
13. Samuel, W., Masliah, E., Hill, L.R., Butters, N. and Terry, R. (1994) Hippocampal connectivity and Alzheimer's dementia: effects of synapse loss and tangle frequency in a two-component model. *Neurology*, **44**, 2081–2088.
14. Schater, D.L. (1996) *Searching for Me*. Basic Books, New York, NY.
15. Maguire, E.A., Gadian, D.G., Johnsrude, I.S., Good, C.D., Ashburner, J., Frackowiak, R.S. and Frith, C.D. (2000) Navigation-related structural change in the hippocampi of taxi drivers. *Proc. Natl. Acad. Sci. U S A*, **97**, 4398–4403.
16. Peigneux, P., Laureys, S., Fuchs, S., Collette, F., Perrin, F., Reggers, J., Phillips, C., Degueldre, C., Del Fiore, G., Aerts, J. *et al.* (2004) Are spatial memories strengthened in the human hippocampus during slow wave sleep? *Neuron*, **44**, 535–545.
17. Davis, J.B. and Maher, P. (1994) Protein kinase C activation inhibits glutamate-induced cytotoxicity in a neuronal cell line. *Brain. Res.*, **652**, 169–173.
18. Morimoto, B.H. and Koshland, D.E. Jr. (1990) Induction and expression of long- and short-term neurosecretory potentiation in a neural cell line. *Neuron*, **5**, 875–880.
19. Manczak, M., Kandimalla, R., Yin, X. and Reddy, P.H. (2018) Hippocampal mutant APP and amyloid beta induced cognitive decline, dendritic spine loss, defective autophagy, mitophagy and mitochondrial abnormalities in a mouse model of Alzheimer's disease. *Hum. Mol. Genet.*, **27**, 1332–1342.
20. Manczak, M., Mao, P., Calkins, M.J., Cornea, A., Reddy, A.P., Murphy, M.P., Szeto, H.H., Park, B. and Reddy, P.H. (2010) Mitochondria-targeted antioxidants protect against amyloid-beta toxicity in Alzheimer's disease neurons. *J. Alzheimers Dis.*, **20**, S609–S631.
21. Calkins, M.J., Manczak, M., Mao, P., Shirendeb, U. and Reddy, P.H. (2011) Impaired mitochondrial biogenesis, defective axonal transport of mitochondria, abnormal mitochondrial dynamics and synaptic degeneration in a mouse model of Alzheimer's disease. *Hum. Mol. Genet.*, **20**, 4515–4529.
22. Manczak, M., Calkins, M.J. and Reddy, P.H. (2011) Impaired mitochondrial dynamics and abnormal interaction of amyloid beta with mitochondrial protein Drp1 in neurons from patients with Alzheimer's disease: implications for neuronal damage. *Hum. Mol. Genet.*, **20**, 2495–2509.
23. Manczak, M., Anekonda, T.S., Henson, E., Park, B.S., Quinn, J. and Reddy, P.H. (2006) Mitochondria are a direct site of A beta accumulation in Alzheimer's disease neurons: implications for free radical generation and oxidative damage in disease progression. *Hum. Mol. Genet.*, **15**, 1437–1449.

24. Reddy, P.H. and Beal, M.F. (2008) Amyloid beta, mitochondrial dysfunction and synaptic damage: implications for cognitive decline in aging and Alzheimer's disease. *Trends Mol. Med.*, **14**, 45–53.
25. Anandatheerthavarada, H.K., Biswas, G., Robin, M.A. and Avadhani, N.G. (2003) Mitochondrial targeting and a novel transmembrane arrest of Alzheimer's amyloid precursor protein impairs mitochondrial function in neuronal cells. *J. Cell Biol.*, **161**, 41–54.
26. Kandimalla, R., Manczak, M., Yin, X., Wang, R. and Reddy, P.H. (2018) Hippocampal phosphorylated tau induced cognitive decline, dendritic spine loss and mitochondrial abnormalities in a mouse model of Alzheimer's disease. *Hum. Mol. Genet.*, **27**, 30–40.
27. Sheng, B., Wang, X., Su, B., Lee, H.G., Casadesus, G., Perry, G. and Zhu, X. (2012) Impaired mitochondrial biogenesis contributes to mitochondrial dysfunction in Alzheimer's disease. *J. Neurochem.*, **120**, 419–429.
28. Qin, W., Haroutunian, V., Katsel, P., Cardozo, C.P., Ho, L., Buxbaum, J.D. and Pasinetti, G.M. (2009) PGC-1alpha expression decreases in the Alzheimer disease brain as a function of dementia. *Arch. Neurol.*, **66**, 352–361.
29. Du, H., Guo, L., Yan, S., Sosunov, A.A., McKhann, G.M. and Yan, S.S. (2010) Early deficits in synaptic mitochondria in an Alzheimer's disease mouse model. *Proc. Natl. Acad. Sci. U S A*, **107**, 18670–18675.
30. Caccamo, A., De Pinto, V., Messina, A., Branca, C. and Oddo, S. (2014) Genetic reduction of mammalian target of rapamycin ameliorates Alzheimer's disease-like cognitive and pathological deficits by restoring hippocampal gene expression signature. *J. Neurosci.*, **34**, 7988–7998.
31. Oddo, S. (2012) The role of mTOR signaling in Alzheimer disease. *Front. Biosci. (Schol Ed)*, **4**, 941–952.
32. Reddy, P.H., Manczak, M., Yin, X., Grady, M.C., Mitchell, A., Kandimalla, R. and Kuruva, C.S. (2016) Protective effects of a natural product, curcumin, against amyloid β induced mitochondrial and synaptic toxicities in Alzheimer's disease. *J. Investig. Med.*, **64**, 1220–1234.
33. Manczak, M., Kandimalla, R., Fry, D., Sesaki, H. and Reddy, P.H. (2016) Protective effects of reduced dynamin-related protein 1 against amyloid beta-induced mitochondrial dysfunction and synaptic damage in Alzheimer's disease. *Hum. Mol. Genet.*, **25**, 5148–5166.